www.lpr-journal.org Vol. 7 No. 2 March 2013

LASER & PHOTONICS REVIEWS

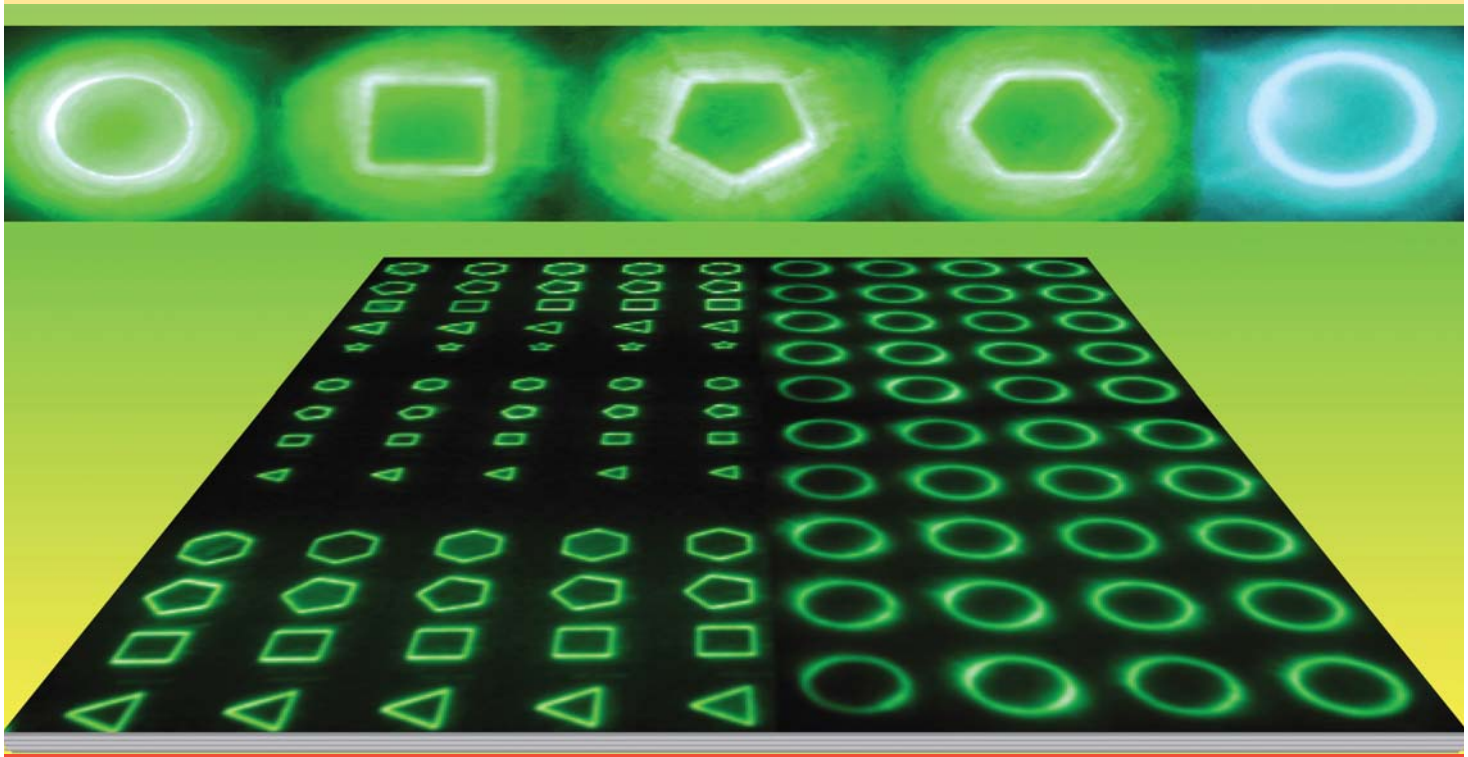

Whispering-gallery mode lasing from patterned molecular single-crystalline microcavity array

Organic single-crystalline materials have attracted great attention for laser applications. However, the fabrication of laser resonators and patterns of crystals is still an intractable problem. Organic single crystals have been limited to fundamental property studies despite their superior photonic characteristics. In this work by **Hong-Hua Fang et al. (p. 281–288),** whispering-gallery mode (WGM) resonators of BP1T and BP2T crystalline materials have been fabricated through a combination method with improved lithography and dry etching. Crystalline microresonators with different geometries over a large area are top-down fabricated with submicrometer spatial resolution. WGM lasing oscillation from circular, hexagonal, pentagonal and square resonators are definitively observed. The BP1T and BP2T crystals are characterized with high refractive index, and stable lasing in aqueous solution is demonstrated besides in the air environment. It is expected that organic crystalline materials would be used for the practical applications in a variety of organic electronic and optical devices.

WILEY-VCH

Laser Photonics Rev. **7,** No. 2, 281–288 (2013) / **DOI** 10.1002/lpor.201200072

LASER & PHOTONICS REVIEWS

Abstract Organic single-crystalline materials have attracted great attention for laser applications. However, the fabrication of laser resonators and pattern of crystals are still intractable problems. Organic single crystals have been limited to fundamental property studies despite their superior photonic characteristics. In this work, whispering-gallery mode (WGM) resonators of BP1T and BP2T crystalline materials have been fabricated through a combination method with improved lithography and dry etching. Crystalline microresonators with different geometries over a large area are top-down fabricated with submicrometer spatial resolution. WGM lasing oscillation from circular, hexagonal, pentagonal and square resonators is definitively observed. The BP1T and BP2T crystals are characterized with high refractive index, and stable lasing in aqueous solution is demonstrated besides in the air environment. It is expected that organic crystalline materials would be used for the practical applications in a variety of organic electronic and optical devices.

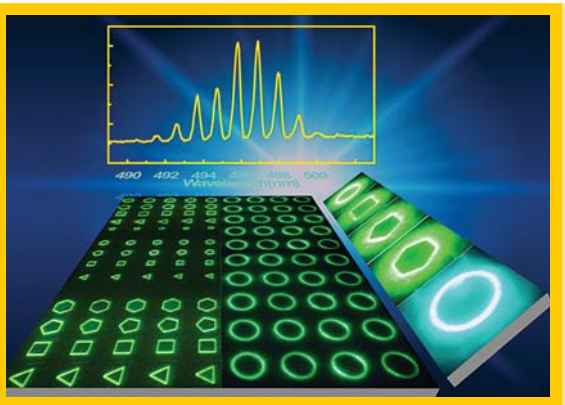

ORIGINAL PAPER

Whispering-gallery mode lasing from patterned molecular single-crystalline microcavity array

Hong-Hua Fang[1], Ran Ding[1], Shi-Yang Lu[2], Yue-De Yang[3], Qi-Dai Chen[1], Jing Feng[1,*], Yong-Zhen Huang[3], and Hong-Bo Sun[1,2,*]

1. Introduction

Organic single crystals have excited great interest as active building materials for electronic and photonic devices [1–5]. Compared to their inorganic counterparts, organic materials offer several advantages, such as inherent compatibility with plastic substrates, flexibility, and amenability to low-cost and low-temperature processing. Spectral narrow emission or amplified spontaneous emission has been observed in several organic crystals [6–11]. The ordered molecular packing, absence of grain boundaries and minimized concentration of charge traps in crystals make them superior in electronic properties (e.g. high mobility, up to 20 $cm^2\ V^{-1}\ s^{-1}$) over polymers, which could feed renewed optimism that electrically pumped organic lasers might prove feasible [12–14]. High-order molecule packing and purity in crystals are also very favorable to the thermal and photonic properties, e.g. excellent photostability, self-waveguide and highly polarization states [8, 11]. Furthermore, refractive indices as high as 4.0 have been demonstrated in some crystals, such as thiophene/phenylene co-oligomers [15]. Then, the optical functions can be made ultracompact to miniaturize photonic devices, due to the high refractive index of organic crystals. This is especially important for microphotonic components, such as whispering-gallery mode (WGM) lasers, in which the light is trapped due to total internal reflection at the interface [16].

As essential components in photonic circles, WGM microresonators provide irreplaceable device geometry for realizing ultracompact laser source. They are in high demand for many applications, such as sensing, filtering, quantum information processing, and on-chip photonics integration [17–28]. In the past decade, organic semiconductor thin-film WGM microcavities, such as microdisk, microcone, and microrings have been developed for application in integrated photonic devices. However, compared to their thin-film counterparts, organic semiconductor single-crystalline microresonators have been produced and patterned with limited success because of the difficulty in the device fabrication, which strongly relies on the availability of high-quality single crystals of suitable dimensions and shape

[1] State Key Laboratory on Integrated Optoelectronics, College of Electronic Science and Engineering, Jilin University, 2699 Qianjin Street, Changchun, 130012, China
[2] College of Physics, Jilin University, 119 Jiefang Road, Changchun, 130023, China
[3] State Key Laboratory on Integrated Optoelectronics, Institute of Semiconductors, Chinese Academy of Sciences, Beijing, China
*Correspondence author(s): e-mail: jingfeng@jlu.edu.cn, hbsun@jlu.edu.cn

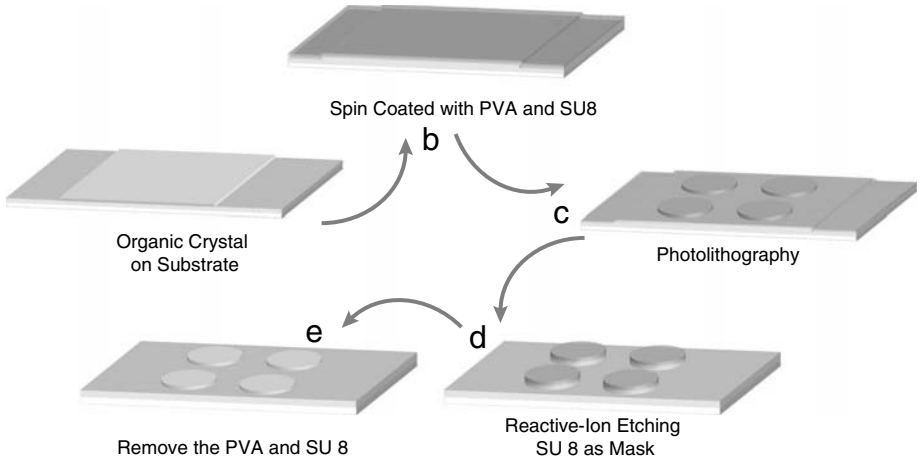

Scheme 1 (online color at: www.lpr-journal.org) Schematic illustration of organic crystal microdisk fabrication process. (a) The grown thin-film crystal is transferred onto the substrate. (b) Then the organic crystal was spin coated with polyvinyl alcohol (PVA) and SU-8 photoresist. (c) UV-exposure and development of SU-8 photoresist. (d) Optimized pattern transfer by reactive-ion etching (RIE). (e) Remove the PVA and resist.

[6, 29, 30]. Furthermore, the crystals are generally fragile and delicate, and hence cannot be processed and simply patterned as can inorganic semiconductors. Due to these reasons, organic single-crystal devices have been traditionally limited to fundamental property studies despite their superior photonic characteristics. To overcome these issues, it simultaneously requires both easy realization of high-quality single-crystalline resonators and the patterning of these cavities over a large area with a high spatial resolution at the submicrometer level.

In this work, we report the fabrication of large microdisk arrays of single crystals and observed whispering-gallery mode lasing from these microresonators. By using an improved lithography technique, patterned microresonators with different geometry are top-down created. Whispering-gallery mode lasing oscillation is unambiguously observed from circular, hexagonal, pentagonal and square resonators. Size- and thickness-dependent investigations on the WGM lasing characteristics are also carried out systematically. Lasing features are not only dependent on the shape size, but also the disk thickness. The investigated crystalline cavities are characterized with high refractive index, and lasing in aqueous solution is also demonstrated in the air environment. To the best of our knowledge, this is the first report on whispering-gallery mode lasing from patterned organic crystalline microresonators with a submicrometer spatial resolution.

2. Results and discussions

2.1. Patterning of crystalline microdisk array

Scheme 1 depicts a schematic diagram for the fabrication process of microdisk array. The microdisk array was fabricated based on the crystalline thin film, which is grown by physical vapor transport in a flowing stream of argon [31]. The BP2T and BP1T crystals (see its structural formula in inset of Scheme 2), representative of thiophene/phenylene co-oligomers (TPCOs), were chosen in the experiment, because of their excellent electronic and optical functionalities [32–34]. The fluorescence lifetime for BP1T and the BP2T crystal is 0.77 ns and 1.14 ns, respectively, according to the time-correlated single-photon counting measurement. The quantum yield for BP1T and BP2T crystal, determined with an integrating sphere, is 36% and 59%, respectively. They have a large cross section of the order of 10^{-16} cm^2 (see Supporting Information). The physical vapor transport method enables us to grow high-quality large-size crystals. The surface roughness for thin film crystals is at the molecular level, and then the mechanical polishing process is avoided. A protection layer polyvinyl alcohol (PVA) film, which is resistant to most organic solvents, is spin coated on top of the thin crystalline before the fabrication process. We have patterned microdisks of various geometries using a nonstandard photolithography. The soft-bake and

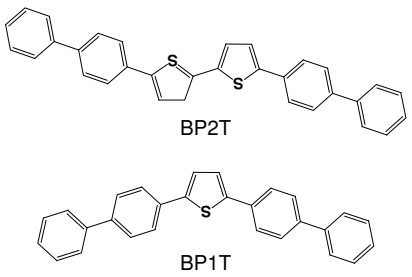

Scheme 2 Chemical structure of BP2T and BP1T.

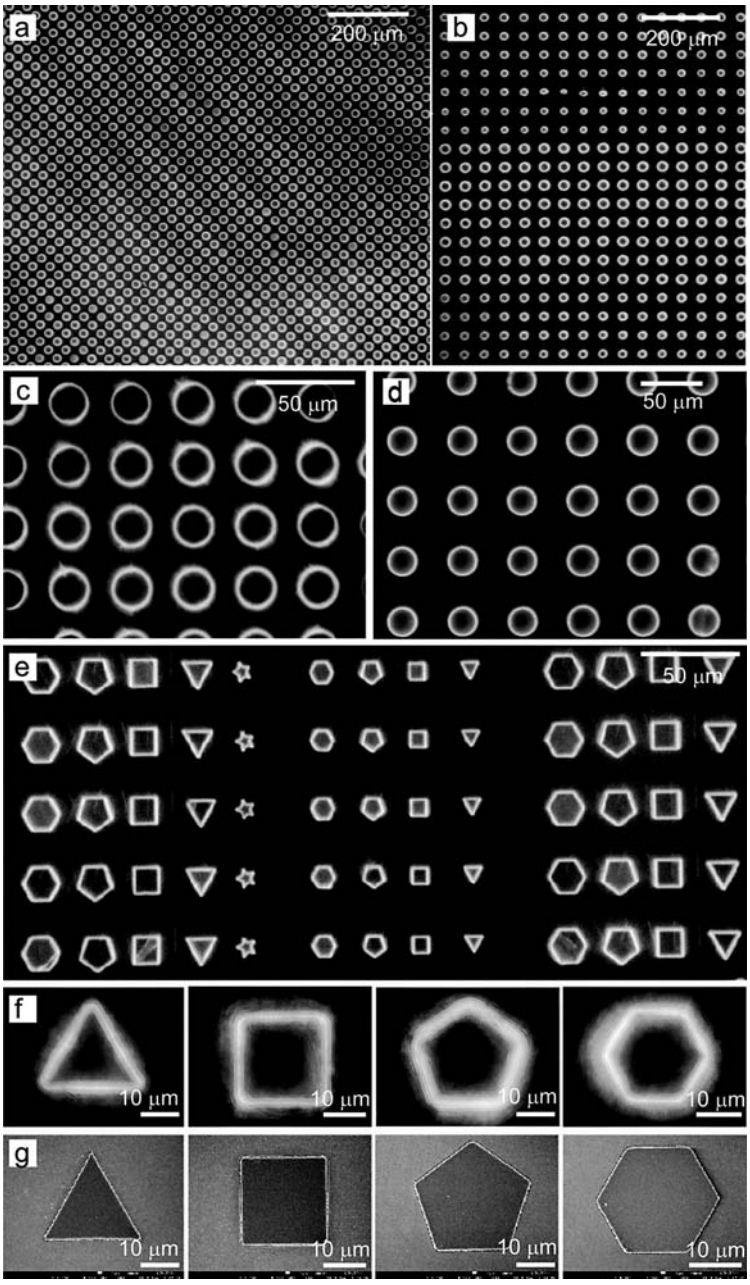

Figure 1 (online color at: www.lpr-journal.org) Patterned crystalline microdisk array. Fluorescence photograph of circle (a, c) BP2T and (b, d) BP1T microdisk. (e, f) Fluorescence photograph of fabricated polygon BP2T microdisk arrays, including triangular, square, pentagonal, hexagonal and star. (g) Scanning electron microscope image of individual polygon BP2T microdisk.

postexposure bake temperatures were kept below 70 °C in order to avoid cracking, which may be induced by uneven distribution of stress in a crystal during the bake process. The microdisk pattern was then transferred to the crystal by reactive-ion etching (RIE). The disks of photoresist act as an etch mask during this dry-etch process. The remaining resist was then wiped off with SU8 remover, and PVA protection layer on the crystal selectively dissolved in aqueous solution.

The fabricated crystal microdisk arrays, imaged using a fluorescence microscope, are shown in Fig. 1. From these images, it can be seen that ordered arrays of semiconductor features with different sizes and shapes, such as circles, hexagons, pentagons, squares, etc., can be obtained over relatively large areas. The magnified images in the insets show that the patterned films have well-defined edges and are located on a clean background. Under UV excitation, bright lights are clearly observed at edge of disks, indicating

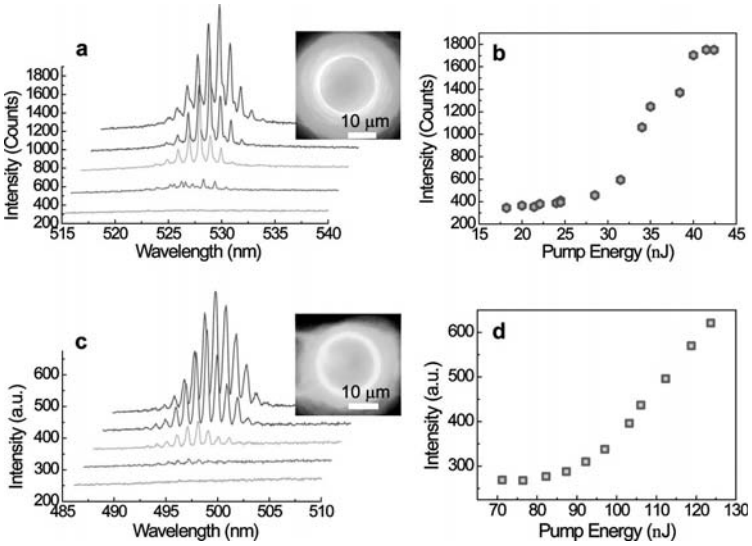

Figure 2 (online color at: www.lpr-journal.org) Lasing characteristics of circular microdisks. (a) The PL spectrum recorded at different pump energy for a BP2T circle microdisk. (b) Superlinear dependence of the emitted intensity of one selected WGM lasing peak on the pump intensity. (c) The PL spectrum recorded at different pump energy for a BP1T circle microdisk. (d) Superlinear dependence of the emitted intensity on the pump intensity.

that the PL emission can be confined and waveguided in the disks. This method is reproducible with high yield at least for BP1T and BP2T crystals, which is very important for future integrated photonics applications. The shape and number of disks is dependent on the size of the used crystal and defined pattern of mask. SEM images of individual polygonal microdisks (triangular, square, pentagonal and hexagonal structures) also demonstrate well-defined shape.

2.2. Lasing characteristics of circle microdisks

To investigate the optical properties of patterned microdisk arrays, photoluminescence from disks was studied one by one (see Supporting Information). Figure 2a depicts the μ-PL spectra from a BP2T circle disk (images attached in inset of Fig. 2a). It can be seen that the PL intensity increases with increasing pump energy of the incident laser, and sharp peaks located at around 525 nm emerge from the emission spectrum when the pump power exceeds a certain value (32 nJ). The evolution from spontaneous to stimulated emission can be seen very clearly. As input power further increased, the lasing mode becomes stable. In our experiment, single lasing mode was not observed. A possible reason may that the pump power is varied too fast to resolve the change from single lasing mode to multimode. A plot of PL intensity of the peak with excitation density is shown in Fig. 2b. Such a nonlinear increase of the emission intensity further indicates a lasing phenomenon in the microcrystal disk. A similar spectrum was observed in the BP1T microdisk as shown in Fig. 2c, and its threshold is about 88 nJ. To form a stable oscillation in the cavity and make light waves strengthened due to interference, the phase change for the light going a round-trip in the cavity should be an integer multiple of 2π, i.e., the resonance condition [35]:

$$nL = m\lambda \tag{1}$$

where n, L are the phase refractive index of the crystal and round-trip distance, respectively, and m is the order of the mode (an integer). Restricted by the condition, only certain frequencies of light are ultimately chosen and enhanced by the cavity. To analyze the laser spectrum we recall that the spectral spacing $\Delta\lambda$ between adjacent laser modes is given by the following relation:

$$\Delta\lambda = \frac{\lambda^2}{n_g L}, \tag{2}$$

where n_g is the group refractive index that is expressed as follows:

$$n_g = n\left(1 - \frac{\lambda dn}{nd\lambda}\right). \tag{3}$$

The lasing peaks spacing $\Delta\lambda$ of the emission lines in Fig. 3a is about 1.05 nm. Since the fundamental WGM modes are located nearby the circumference of the cavity, $L \approx \pi D$ is used as an approximation in circular disks. Using the emission line at 526.1 nm and a diameter, D of 19 μm, we get from Eq. ((2)) a group refractive index, n_g (526.1 nm) $\approx$ 4.42, which is exceptionally high among organic semiconductor, and comparable to the results of other TPCO crystals [15]. The wavelength dependence of n_g can be determined, which then allows us to calculate the phase refractive index n (see Fig. S2b, Supporting Information). The corresponding mode numbers are indexed as 313–319 (Fig. 3a), matching well with the measured lasing peaks. The measured group refractive index for BP1T near 500 nm is above 4.9, and the phase refractive index is also as high as 2.9.

The characteristics of the WGM lasing action dependent on the geometry size in circular disks were investigated by examining the mode spacing (ΔE). The mode spacing is shown in Fig. 3b, gradually decreasing with

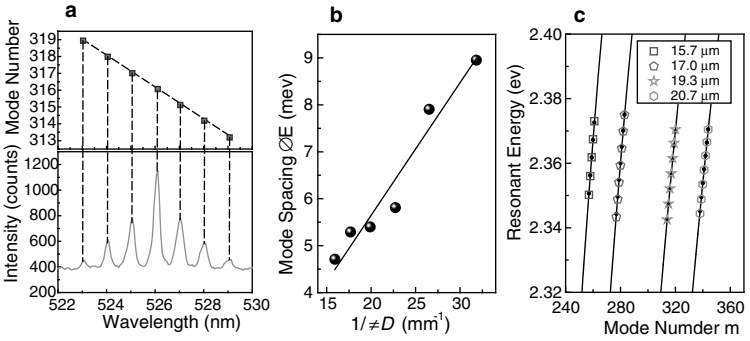

Figure 3 (online color at: www.lpr-journal.org) Mode analysis of circle BP2T microdisks. (a) Lasing spectrum at 34.1 nJ, and calculated WGM lasing mode numbers. (b) The mode spacing as a function of reciprocal of circle disk size. (c) Lasing resonant energy (large symbols) and theoretical fit (line-dot), determined from Eq. ((1)).

increasing disk size. It is found that the experimentally measured mode spacing is proportional to the reciprocal diameter of a circle. In order to get a clearer picture of the mode spacing dependence on the disk diameter, the resonant energy of WGM cavities as a function of mode number m is presented in Fig. 3c. The mode spacing is the spatial distance between lasing peaks (big symbols), which regularly decreases with increasing m, corresponding to the increase of microdisk size. A larger diameter leads to higher interference orders observed in the spectra in the same spectral range. Considering the measurement error of the diameter and the resolution of spectrometer (about 0.06 nm), the calculated value (line–symbols) is in good accordance with the experimental data, which implies that the lasing mechanism from the circle disks is indeed ascribed to WGM.

The Q factor is another important parameter to describe a laser cavity, which is typically used to evaluate the capability of a cavity to store energy. In practice, the Q is determined by $1/Q = 1/Q_{\text{abs}} + 1/Q_{\text{scat}} + 1/Q_{\text{cav.}}$ The first term Q_{abs} is associated with absorption and bulk Rayleigh scattering in the material constituting the microresonator; Q_{scat} describes the losses due to light scattering by surface roughness; and the last term Q_{cav} represents radiative (curvature) losses. It is therefore understood that the Q factor of a WGM resonator is sensitively affected by its surface roughness and shape deformation. From the experiment, the Q factor for the circle disk in Fig. 3a is estimated to be $\sim$2030 according to the spectral parameters $Q = \lambda/\delta\lambda$, where λ is the peak wavelength and the $\delta\lambda$ is the line with of the peak, respectively. There is still much scope to improve the Q factor to further lower the lasing threshold.

The lasing spectrum was further investigated from circular disks with different thickness. When the thickness was less than 500 nm, as mentioned above, lasing oscillation occurred mainly at the region of 520–530 nm (defined as the blue region). When the larger thickness crystals are used in the experiment, the lasing emission in the region around 565 nm appears (defined as the red region). Spectra at different pump level for microdisks with thicknesses of 1 μm and 1.5 μm, are shown in Figs 4a and b, respectively. The lasing modes in the red region are apparent when a high thickness disk is investigated, and the threshold is

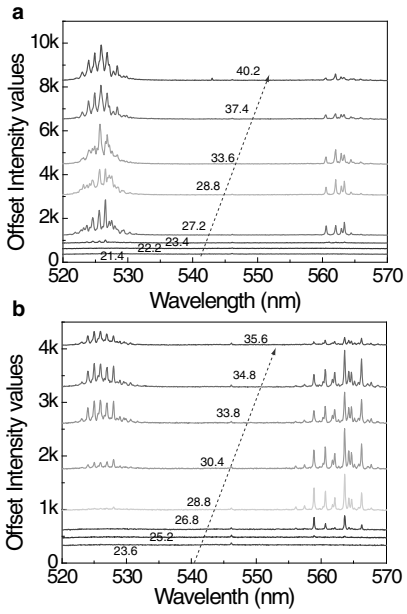

Figure 4 (online color at: www.lpr-journal.org) Lasing spectrum from microdisks with different thickness. (a) Lasing spectra of BP2T circle disk ($\sim$ 20 μm diameter) under different pump energy with thickness about 1 μm. (b) Lasing spectra of BP2T circular disk under different pump energy with thickness about 1.5 μm.

even lower than that of blue region, as shown in Figure 4b. However, these red region lasing modes disappear when the pump energy is further raised. This behavior is very similar with amplified spontaneous emission of BP2T crystal (see Fig. S4, Supporting Information). "two-color" ASE occurs when suitable thickness crystals and pump power are employed. This may be ascribed to the reabsorption by ground-state molecules. For the thick crystals or disks, the large reabsorption effect increased the lasing threshold in the blue region (0–1 transitions), leading to higher threshold than those of the red region (0–2 transitions). However, the gain in the blue region increases rapidly as the pump level

is elevated. This leads to the lasing spectrum in the blue region emerging, and red lasing lines being suppressed. It should be noted that the mode spacing (in the form of $\Delta\lambda$) in the red region is much larger than that in the blue region (Fig. S2a, Supporting Information), which is attributed to the dispersion of refractive indices.

The fabrication of microstructures in crystalline materials and patterning of the device is one of prerequisite conditions for practical applications. The present results clearly show that microdisk arrays with large area could be fabricated with an optimized optical lithography and reactive ion etching processes, and stable lasing oscillation was first demonstrated from single-crystalline microcavities. It is expected that this method is not only suitable for microlaser array fabrication, but also compatible electronic devices, such as patterned organic field-effect transistors (OFETs) for active matrix display and sensor arrays [36, 37].

2.3. WGM lasing from polygonal microresonators

Polygon cavities have recently attracted much attention due to their potential application in photonic integrated circuits and optical interconnects [38, 39]. Polygon cavities may found applications for direction laser source in photonic integrated circuits. The optical properties from polygonal cavities made of BP2T single crystal are further investigated. Lasing oscillations are unambiguously observed in the regular polygonal cavity based on the BP2T crystals, as shown in Fig. 5. These organic crystal microlasers with regular polygonal geometries may be attractive as a coherent light source for miniaturized photonic circuits. It is noted that lasing modes remain located around the region of 520–530 nm, though cavities with different geometries were excited. It is reasonable that lasing occurs in the section with high gain. In a polygonal resonator, the light travels around due to total internal reflection at the resonator boundary, as schematically shown in the insets of Figs. 5a–c for hexagonal, pentagonal and square resonators, respectively. WGMs supported by a polygonal microcavity are intrinsically of multimode. In other words, there exist many eigenmodes satisfying the condition of total internal bounce reflections at the cavity walls, as seen in circular disks. The experimentally determined $\Delta\lambda$ is 0.62 nm for a hexagonal disk and mode numbers are shown in Fig. 5a. The theoretical free spectral range (0.63 nm) is fit well with the experimental data, which confirms the WGM lasing mechanism. The theoretical free spectral ranges for a pentagon and a square approximate to the experimental values, considering the resolution of the spectrometer and measurement error, as shown in Figs. 5b and c. The lasing spectrum for a hexagonal resonator is the sharpest among the polygonal cavities, corresponding to the highest Q factor. The experimental Q factor increases with the increase in the cavity polygonal order. It should be noted that no lasing oscillation was observed in star and triangular geometries.

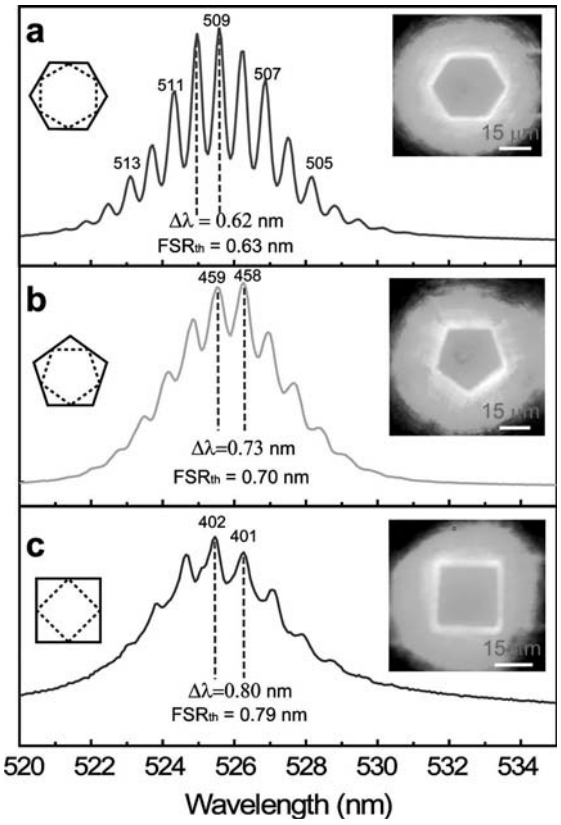

Figure 5 (online color at: www.lpr-journal.org) Lasing spectra from polygon resonators, (a) hexagonal, (b) pentagonal and (c) square microcavities. The corresponding PL images microdisk are shown in the inset of figures.

2.4. Crystalline microresonators in aqueous solution

The BP2T and BP1T microdisks under UV laser excitation show whispering-gallery modes in the air, and the lasing spectra mentioned above are recorded in the air. Moreover, we found that the WGM lasing oscillations survive well in aqueous solution. We record the spectra of a circle microdisk in air and water, respectively (Fig. 6b), with the schematic diagrams showing the difference in the environments (Fig. 6a). Lasing oscillation is also observed in the aqueous environment. To the best of our knowledge, laser action of an organic microcavity has not yet been demonstrated in water. WGM optical microcavities trap light via the total internal reflection at the circular boundary formed between the dielectric cavity and surroundings. With the increase of the refractive index of the surrounding medium, the reflectivity at the boundary between the active materials and the medium will decrease, which leads to a smaller Q and confinement (F) factor, and results in a extremely high WGM lasing threshold, even the disappearance of lasing

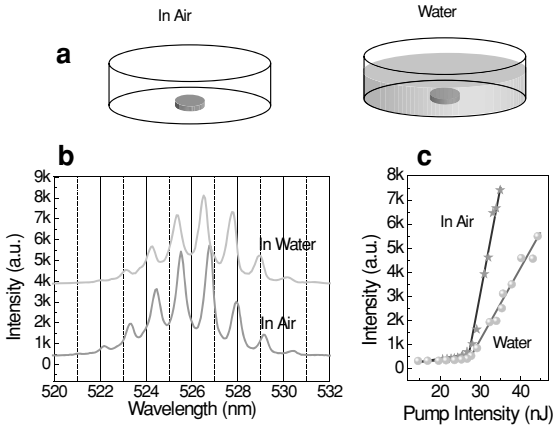

Figure 6 (online color at: www.lpr-journal.org) (a) Schematic diagram for the lasing measurement in air and water solution. (b) Measured spectra of the lasing emission from BP2T crystal microcircle disk ($D \sim 20$ mm) in different environments, air and aqueous solution. (c) Output intensity as a function of the pump energy.

oscillation. Figure 6c plots the emission intensity with the change of excitation density for two measurements. The discrepancy in the spectrum and threshold is not apparent, which may arise from the high refractive index of BP2T crystal as mentioned above.

3. Conclusions

In summary, we have fabricated monolithic small-molecular single-crystalline microlaser arrays with large area on a chip, and laser oscillation was demonstrated in these crystal microcavities. The crystal microlaser may provide an important new feature for chips: feasible plastic devices. These results are promising in view of developing innovative organic lasers and as base components in integrated microphotonics.

Acknowledgements. This work was supported by the Natural Science Foundation of China (NSFC) under Grants #61127010, 90923037, and 61137001.

Supporting information for this article is available free of charge under http://dx.doi.org/10.1002/lpor.201200072.

Received: 25 August 2012, **Revised:** 26 September 2012, **Accepted:** 11 October 2012

Published online: 21 December 2012

Key words: Whispering gallery mode, organic single crystals, lasing, microdisk.

References

[1] Q. H. Cui, Y. S. Zhao, and J. N. Yao, J. Mater. Chem. **22**, 4136–4140 (2012).
[2] K. Takazawa, Y. Kitahama, Y. Kimura, and G. Kido, Nano Lett. **5**, 1293–1296 (2005).
[3] Q. X. Tang, L. Jiang, Y. H. Tong, H. X. Li, Y. L. Liu, Z. H. Wang, W. P. Hu, Y. Q. Liu, and D. B. Zhu, Adv. Mater. **20**, 2947–2951 (2008).
[4] W. J. Xie, Y. P. Li, F. Li, F. Z. Shen, and Y. G. Ma, Appl. Phys. Lett. **90**, 141110 (2007).
[5] C. Grivas and M. Pollnau, Laser Photon. Rev. **6**, 419–462 (2012).
[6] H. H. Fang, R. Ding, S. Y. Lu, J. Yang, X. L. Zhang, R. Yang, J. Feng, Q. D. Chen, J. F. Song, and H. B. Sun, Adv. Funct. Mater. **22**, 33–38 (2011).
[7] D. Fichou, S. Delysse, and J. M. Nunzi, Adv. Mater. **9**, 1178–1181 (1997).
[8] H. Yanagi, T. Ohara, and T. Morikawa, Adv. Mater. **13**, 1452–1455 (2001).
[9] R. Hibino, M. Nagawa, S. Hotta, M. Ichikawa, T. Koyama, and Y. Taniguchi, Adv. Mater. **14**, 119–122 (2002).
[10] M. Ichikawa, R. Hibino, M. Inoue, T. Haritani, S. Hotta, K. Araki, T. Koyama, and Y. Taniguchi, Adv. Mater. **17**, 2073–2077 (2005).
[11] H. H. Fang, Q. D. Chen, J. Yang, H. Xia, Y. G. Ma, H. Y. Wang, and H. B. Sun, Opt. Lett. **35**, 441–443 (2010).
[12] T. Takenobu, S. Z. Bisri, T. Takahashi, M. Yahiro, C. Adachi, and Y. Iwasa, Phys. Rev. Lett. **100**, 066601 (2008).
[13] C. Reese and Z. N. Bao, J. Mater. Chem. **16**, 329–333 (2006).
[14] C. Reese, M. E. Roberts, S. R. Parkin, and Z. A. Bao, Adv. Mater. **21**, 3678–3681 (2009).
[15] T. Yamao, K. Yamamoto, Y. Taniguchi, T. Miki, and S. Hotta, J. Appl. Phys. **103**, 093115 (2008).
[16] A. Chiasera, Y. Dumeige, P. Feron, M. Ferrari, Y. Jestin, G. N. Conti, S. Pelli, S. Soria, and G. C. Righini, Laser Photon. Rev. **4**, 457–482 (2010).
[17] K. J. Vahala, Nature **424**, 839–846 (2003).
[18] D. J. Gargas, M. C. Moore, A. Ni, S. W. Chang, Z. Y. Zhang, S. L. Chuang, and P. D. Yang, ACS Nano **4**, 3270–3276 (2010).
[19] F. Scotognella, D. P. Puzzo, A. Monguzzi, D. S. Wiersma, D. Maschke, R. Tubino, and G. A. Ozin, Small **5**, 2048–2052 (2009).
[20] P. T. Snee, Y. H. Chan, D. G. Nocera, and M. G. Bawendi, Adv. Mater. **17**, 1131–1136 (2005).
[21] Y. Akahane, T. Asano, B. S. Song, and S. Noda, Nature **425**, 944–947 (2003).
[22] A. Camposeo, F. Di Benedetto, R. Stabile, A. A. R. Neves, R. Cingolani, and D. Pisignano, Small **5**, 562–566 (2009).
[23] R. Kirchain and L. Kimerling, Nature Photon. **1**, 303–305 (2007).
[24] S. P. Lau, H. Y. Yang, S. F. Yu, C. Yuen, E. S. P. Leong, H. D. Li, and H. H. Hng, Small **1**, 956–959 (2005).
[25] W. H. Guo, Y. Z. Huang, and Q. M. Wang, IEEE Photon. Technol. Lett. **12**, 813–815 (2000).
[26] J. Ward and O. Benson, Laser Photon. Rev. **5**, 553–570 (2011).
[27] K. Ding and C. Z. Ning, Light Sci. Appl. doi:10.1038/lsa.2012.20.
[28] W. Bogaerts, P. De Heyn, T. Van Vaerenbergh, K. De Vos, S. K. Selvaraja, T. Claes, P. Dumon, P. Bienstman, D. Van Thourhout, and R. Baets, Laser Photon. Rev. **6**, 47–73 (2012).

[29] C. Zhang, C. L. Zou, Y. L. Yan, R. Hao, F. W. Sun, Z. F. Han, Y. S. Zhao, and J. N. Yao, J. Am. Chem. Soc. **133**, 7276–7279 (2011).
[30] Y. S. Zhao, A. D. Peng, H. B. Fu, Y. Ma, and J. N. Yao, Adv. Mater. **20**, 1661 (2008).
[31] Y. Yang, R. Goto, S. Omi, K. Yamashita, H. Watanabe, M. Miyazaki, and Y. Oki, Opt. Exp. **18**, 22080 (2010).
[32] S. Hotta, M. Goto, R. Azumi, M. Inoue, M. Ichikawa, and Y. Taniguchi, Chem. Mater. **16**, 237–241 (2004).
[33] S. Z. Bisri, T. Takenobu, Y. Yomogida, H. Shimotani, T. Yamao, S. Hotta, and Y. Iwasa, Adv. Funct. Mater. **19**, 1728–1735 (2009).
[34] S. Hotta and T. Yamao, J. Mater. Chem. **21**, 1295–1304 (2011).
[35] R. C. Polson, G. Levina, and Z. V. Vardeny, Appl. Phys. Lett. **76**, 3858–3860 (2000).
[36] S. H. Liu, H. A. Becerril, M. C. LeMieux, W. C. M. Wang, J. H. Oh, and Z. N. Bao, Adv. Mater. **21**, 1266–1270 (2009).
[37] H. M. Lee, J. J. Kim, J. H. Choi, and S. O. Cho, ACS Nano **5**, 8352–8356 (2011).
[38] A. K. Bhowmik, Appl. Opt. **39**, 3071–3075 (2000).
[39] W. H. Guo, Y. Z. Huang, Q. Y. Lu, and L. J. Yu, IEEE J. Quantum Electron. **39**, 1106–1110 (2003).

